



OPEN

In-situ $\delta^{18}\text{O}$ and $^{87}\text{Sr}/^{86}\text{Sr}$ proxies in an unconformable clastic unit at the Ordovician–Silurian transition

Chaewon Park¹, Yungoo Song^{1✉}, Namsoo Kim¹, Sung-Ja Choi², Ueechan Chwae², Yirang Jang³, Sanghoon Kwon¹, Jeongmin Kim⁴, Ha Kim¹ & Youn-Joong Jeong⁴

Clastic successions found in the carbonate platform of continental margin during the Ordovician–Silurian Transition (OST) period are archives for interpreting paleo-depositional systems. Here, we report in-situ $\delta^{18}\text{O}_{\text{quartz}}$ and $^{87}\text{Sr}/^{86}\text{Sr}_{\text{carbonate}}$ isotope chemo-stratigraphy for an unconformable clastic unit from the Cathaysia terrane that rifted off the Gondwana Supercontinent in the Early Paleozoic Era. Our results suggest a depositional proxy and model for geological events attributed to rapid changes in the sedimentary environment during the OST period. Importantly, these results present crucial clues that infer the influence of Paleo-Tethys Sea opening, global eustatic regression, and rapid sedimentary provenance change. Our study provides insight into paleo-tracer that could be a key method for interpreting depositional system of carbonate platform based on in-situ mineral isotope chemo-stratigraphy that preserves the original value of provenance and geochemical condition.

The Ordovician–Silurian transition (OST) is a period of global upheaval. Above all, a big biota mass extinction event occurred that wiped out up to 60% of the marine genera¹. One of the main factors of global environmental change that led to this cataclysm was the global glaciation that started in Antarctica and reached its maximum during the Hirnantian stage of the Latest Ordovician^{2–6}. This event caused major changes not only in the biosphere but also in the lithosphere. In particular, the global eustatic regression caused by this glaciation greatly increased the continental free board in Gondwana Supercontinent, Baltica, Laurentia, and Siberia^{7,8}, which may have resulted in a depositional transition due to rapid change in the sedimentary environment and the provenance. The clastic successions of OST found between marine sedimentary sequences in the margins of each continent may be a geological proxy related to these changes (Fig. 1a).

The OST carbonate platform found in each continent's marginal environment is a key archive of a paleo-depositional system with a record of geological changes (Fig. 1a). The characteristics of each regional OST clastic unit are summarized as follows (Supplementary Table 1): (1) a wide range of terrigenous lithofacies, from conglomerate to sandstone mixed with carbonate rock in clastic sequences, (2) in general, unconformably overlying the carbonate rock unit that was formed in a marginal shallow marine environment, and (3) conformably underlying another carbonate rock unit. Here, it suggests that two main factors may have contributed: (1) eustatic regression by global glaciation in the Late Ordovician period would have contributed to their creation process, and (2) regional increases in the continental free board would have derived from uplifting by tectonic events.

One of the key tectonic events of the OST period was the Cathaysia terrane's breaking-off from the Gondwana and the subsequent Paleo-Tethys Sea opening^{7–9} (Fig. 1b). This would have provided a compressive stress field on the eastern margin of the Cathaysia terrane resulting in tectonic uplifting and the subsequent increase of continental freeboard. A unique clastic unit formed during the OST period was also found in this area (Fig. 1b and c). It is highly likely that this clastic unit was affected by this tectonic event along with worldwide glaciation during its creation.

Despite previous studies on the clastic successions of the OST period (Fig. 1a), the results based on descriptive approaches did not provide any direct evidence of a change in the provenance of these clastic units. A number of studies through stable isotope analysis have also been attempted^{10–14}, but there were difficulties in separating

¹Department of Earth System Sciences, Yonsei University, Seoul, Republic of Korea. ²Korea Institute of Geoscience and Mineral Resources (KIGAM), Daejeon, Republic of Korea. ³Department of Earth and Environmental Sciences, Chonnam National University, Gwangju, Republic of Korea. ⁴Korea Basic Science Institute (KBSI), Cheongju, Republic of Korea. ✉email: yungoo@yonsei.ac.kr

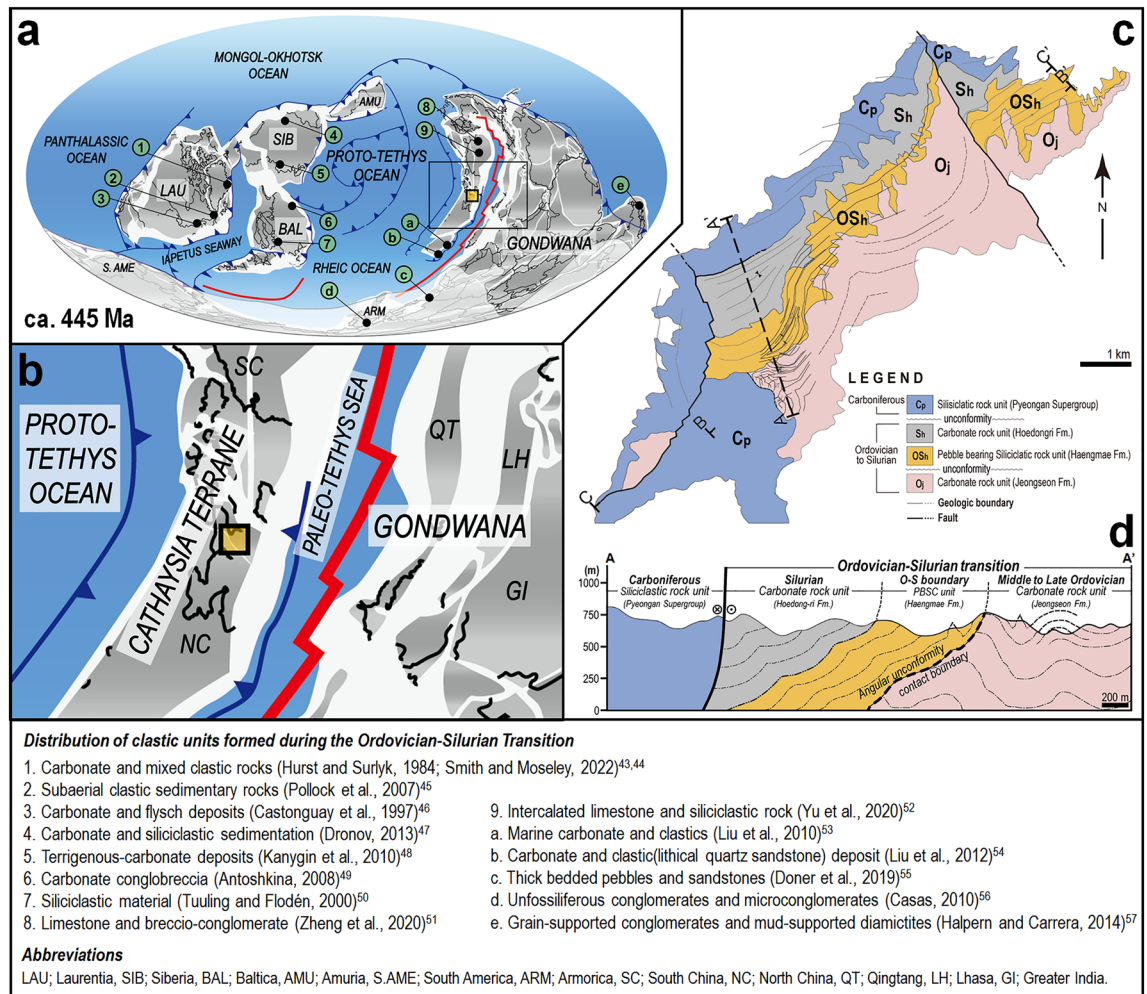


Figure 1. Global creation of clastic units during the Ordovician–Silurian Transition (OST). (a) Reconstruction of a global paleogeographic map (ca. 445 Ma) (modified after refs.^{7–9}) showing the distribution of clastic O-S boundary strata (Supplementary Table 1). (b) Cathaysia terrane's breaking-off from the Gondwana and subsequent Paleo-Tethys Sea opening. Yellow solid square indicates the study area. (c) Simplified geologic map of the study area showing the distribution of clastic succession. The target unit is a pebble-bearing fine sand-sized clastic rock (PBSC) unit, which is in unconformable contact with the underlying carbonate unit. (d) Interpretative A–A' cross-section of the study area. It shows that the PBSC and the underlying carbonate units are unconformable. Figures were drawn using Adobe Illustrator CS6 version 16.0.0 (<https://www.adobe.com/>) and Microsoft PowerPoint Office 365 ProPlus version (<https://www.microsoft365.com/>).

the target mineral from the whole rock sample and overcoming the limitations of the resulting analysis precision and accuracy. The recent progress of in-situ technique has been able to determine the isotopes for several tens of micro-sized minerals in sedimentary rock, while preserving the micro-texture. Since the stable isotopic feature of minerals reflects the chemical conditions of their formation, the in-situ isotopic analyses of minerals can precisely identify some changes in their provenance. In this study, we studied a carbonate platform developed along the margin of a Cathaysia terrane rifted off the Gondwana continent (Fig. 1c and d). We firstly conducted in-situ $\delta^{18}\text{O}_{\text{quartz}}$ and $^{87}\text{Sr}/^{86}\text{Sr}_{\text{carbonate}}$ isotope chemo-stratigraphy on clastic mineral (quartz) and carbonate minerals (calcite and dolomite) in the sedimentary succession of the OST period. Through this, we tried to find out whether the in-situ isotope chemo-stratigraphic proxy indicates the change in the provenance of detrital materials in the clastic unit, and furthermore, whether this becomes a decisive clue to infer the influence of global eustatic regression and Paleo-Tethys Sea opening during the OST period.

Results

An unconformable clastic unit in Gondwana. The study target is a unique clastic unit of the OST period appearing among sedimentary successions of carbonate rocks in the Korean Peninsula. This area was located in the Cathaysia terrane, the northwestern margin of the Gondwana during the Early Paleozoic Era (Fig. 1a and b). It is currently located on the eastern margin of the North China Block (Sino-Korean Block)^{15,16} (Supplementary Fig. 1a). In the previous study, the authors reported the distribution of this target unit through precise mapping¹⁷. A revised version of the geological map is presented (Fig. 1c; Supplementary Fig. 1).

The clastic unit, the so-called Haengmae Formation, is a unique pebble-bearing fine sand-sized clastic rock (PBSC) unit with a layer thickness of about 100 m, which is vulnerable to weathering and forms a gentle topography (Figs. 1c, d, 2a, and b). The PBSC unit covers the lower carbonate unit (Jeongseon Fm.), which is mainly composed of gray limestone and is covered by the upper carbonate unit (Hoedongri Fm.), which mainly consists of packstone and wackestone¹⁷. The PBSC unit generally maintains low-angle bedding with an inclination of less than 15°. Although some folding structures appear, overlapping folding is not observed in the PBSC unit¹⁷ (Fig. 2a; Supplementary Fig. 2).

In contrast, the bedding plane of the lower carbonate unit shows a moderately inclined slope, and its trajectory shows an S-shaped overlapping fold (F2)¹⁷ (Supplementary Fig. 3). This indicates that this unit has undergone at least two-time deformation events. The distinct difference in deformation structure characteristics between the PBSC and the lower carbonate units can be reasonably inferred that there was a large temporal gap between the two strata. In this study, we found several new evidences in the outcrop to confirm the above inference. Above all, the angular unconformity contact between the PBSC and the lower carbonate units was first discovered in the outcrop (Fig. 2f). In addition, the ‘Karst’ surface was found on the uppermost subsurface of the lower carbonate rock unit, which is directly connected to the PBSC unit (Fig. 2g; Supplementary Fig. 4). This is a clear geological signature indicating that the carbonate unit was exposed and denuded on the surface by uplifting through deformation after deposition.

Age constraints for PBSC unit. The deposition period of the PBSC unit could be inferred through U–Pb age dating of the detrital zircon. The results of this study and previous studies are summarized in Supplementary Table 5. Jang¹⁸ reported 449.5 ± 1.5 Ma ($n = 18$) with high reliability as the maximum deposition age of the PBSC unit. The frequency graph (Supplementary Fig. 7) combining data from this study and previous studies^{17,18} strongly indicates that the PBSC unit was deposited during at least the Late Ordovician or Early Silurian period, that is, the OST period.

Macro-/micro-textural features of PBSC unit. The PBSC unit shows the macro-textural characteristics of a typical clastic rock with a granular matrix containing detrital pebbles of various rock types, including dolomite pebbles ranging in size from several mm to several cm¹⁷ (Fig. 2b and c; Supplementary Fig. 5). Dolomite pebbles with gray-brown to yellow–brown fine-grained (10–20 μm) aggregates are predominant in the pebbles. Small amounts of pebbles of micritic mudstone, quartzite, sandstone, and phyllite are included, and white phengite series aggregates ranging in size from several mm to several cm also appear¹⁹. The PBSC unit was partially deformed, and some dolomite pebbles were elongated, showing a shearing sense (Fig. 2b; Supplementary Fig. 5).

The PBSC unit matrix confirmed by XRD and SEM–BSE observation consists of quartz, single-crystalline dolomite, calcite cement, polycrystalline phengite series aggregates, and rock fragments with a size of less than 2 mm (Fig. 2d and e; Supplementary Fig. 5 and Table 2). In our previous micro-textural study, we defined only clastic quartz and rock fragments as sediments in the syn-depositional stage among the constituents of the PBSC unit matrix, and the other minerals as secondary phases formed in the post-depositional stage^{17,19}. Based on these mineral compositions and micro-texture characteristics, the PBSC unit is inherently a typical clastic rock unit and appears to have undergone several post-depositional events.

In-situ $\delta^{18}\text{O}_{\text{quartz}}$ and $^{87}\text{Sr}/^{86}\text{Sr}_{\text{carbonate}}$ chemo-stratigraphic proxies. We conducted in-situ isotope chemo-stratigraphic studies on the PBSC unit and two carbonate rock units (Fig. 3; Supplementary Tables 3 and 4).

Quartz Based on SEM–BSE image observation, quartz, which is the target of in-situ $\delta^{18}\text{O}$ analysis, shows micro-textural characteristics of typical clasts such as various grain sizes, poor sorting, and subangular shape in both PBSC (Supplementary Fig. 5) and carbonate (Supplementary Fig. 6) units. In particular, the quartz content increases rapidly in the PBSC unit, which clearly shows that there was an influx of a large amount of terrestrial clasts (Fig. 3). In in-situ oxygen isotope analysis of detrital quartz, the $\delta^{18}\text{O}_{\text{quartz}}$ values (17.55–23.65 ‰) in the PBSC unit is significantly lower than those of the two carbonate units (23.56–27.01 ‰) (Fig. 3). Since quartz is resistant to secondary alteration^{10,20}, its primary isotope values can be preserved and used as a paleo-tracer for provenance interpretation. Therefore, the sharp drop of $\delta^{18}\text{O}_{\text{quartz}}$ values in the PBSC unit strongly indicates that the provenance of quartz in this unit was clearly changed.

Carbonates The in-situ $^{87}\text{Sr}/^{86}\text{Sr}$ isotope values of carbonate minerals reflect the geochemical conditions of the syn-, or post-depositional stage^{21–24}. In the PBSC unit, the in-situ $^{87}\text{Sr}/^{86}\text{Sr}_{\text{dolomite}}$ values of clastic dolomite pebble (fine-grained dolomite aggregate) fluctuate markedly from 0.7085 to over 0.7149 (Fig. 3). Considering that the carbonate successions in the study area were placed in the same geochemical environment after deposition, this suggests that the clastic dolomite pebbles were formed under geochemical conditions with distinct differences in $^{87}\text{Sr}/^{86}\text{Sr}$ isotope values, and its provenance was different from that of other carbonates.

In the $^{87}\text{Sr}/^{86}\text{Sr}_{\text{dolomite}}$ vs. 1/Sr correlation, the trend of all $^{87}\text{Sr}/^{86}\text{Sr}_{\text{dolomite}}$ values converged to about 0.7084 (Fig. 4a). This indicates that there was an effect of hydrothermal fluid after deposition²³, and the creation of phengite series in the PBSC unit also supports it^{17,19}. This trend of the clastic dolomite pebble shows a completely different pathway from the trend of the single dolomite in the upper and lower carbonate units (Fig. 4a). The $^{87}\text{Sr}/^{86}\text{Sr}_{\text{dolomite}}$ ranged from 0.7095 to 0.7106 according to the Sr variation of the carbonate rock unit (0.0008 to 0.0107). The dolomite pebble of the PBSC unit shows a large variation, with $^{87}\text{Sr}/^{86}\text{Sr}_{\text{dolomite}}$ ranging from 0.7085 to 0.7149 according to Sr variation (0.002–0.0031). This indicates that the clastic dolomite pebble was introduced from a provenance in which the initial $^{87}\text{Sr}/^{86}\text{Sr}_{\text{dolomite}}$ values was distinctly different, and was subsequently reset due to the influence of post-depositional hydrothermal influx.

In the calcite cement of the PBSC unit and calcite of the upper and lower carbonate rock units, there was no significant change in the in-situ $^{87}\text{Sr}/^{86}\text{Sr}_{\text{calcite}}$ values (Fig. 3). It behaves within a similar range (within the

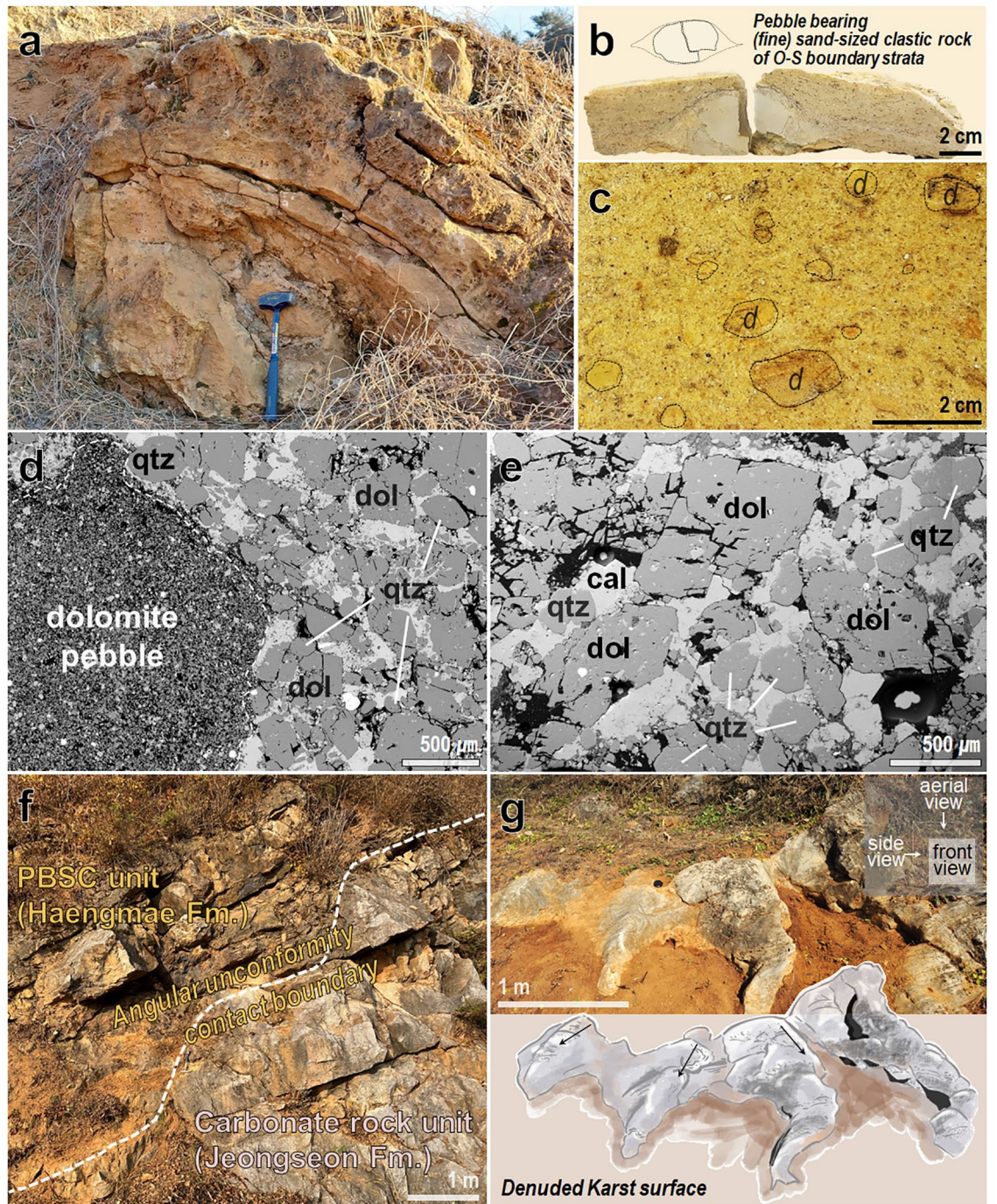


Figure 2. Compilation of outcrop, lithological, and micro-textural characteristics of the PBSC and carbonate rock units. (a) Photograph of a yellowish-brown PBSC unit (Haengmae Fm.) outcrop. (b) Polished slab of elongated dolomite pebble (aggregates of fine-grained dolomite with 10–20 μm in size) by shearing in the PBSC unit. (c) Polished slab showing the macro-textural characteristics of the PBSC unit containing pebbles of various rock types, including dolomite pebbles 'd' ranging in size from a few mm to several cm. (d–e) SEM-BSE image showing the micro-textural features of the PBSC unit. It contains dolomite pebble of several millimeters or more, fine sand-sized quartz (qtz) and dolomite (dol) single grains, and calcite cement that fill the pore space. (f) Outcrop showing the angular unconformity contact boundary between the PBSC and the lower carbonate units. (g) The denuded 'Karst' surface and its sketch at the uppermost subsurface of the carbonate unit (Jeongseon Fm.) below the PBSC unit.

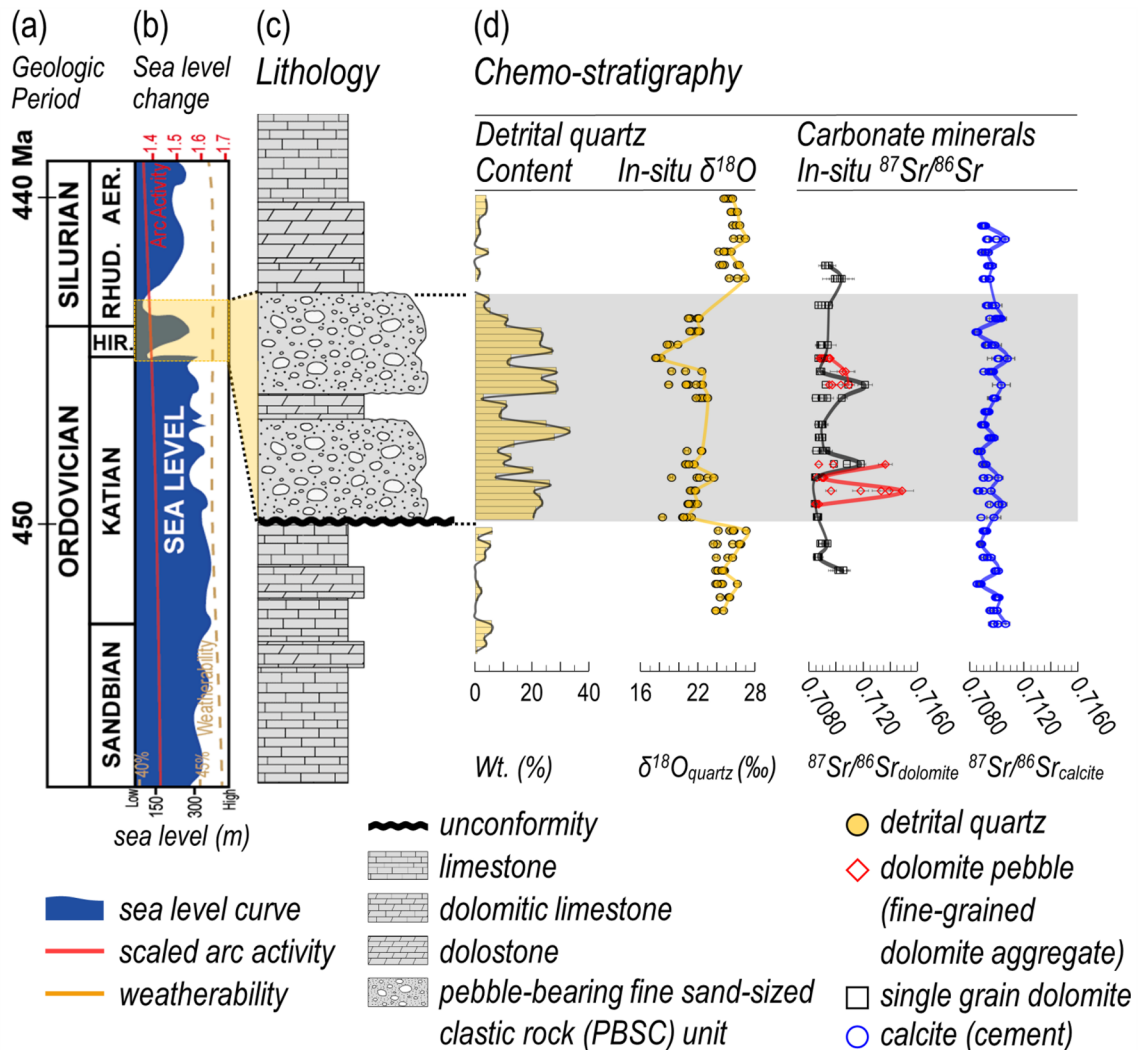


Figure 3. High-resolution in-situ $\delta^{18}\text{O}_{\text{quartz}}$ and $^{87}\text{Sr}/^{86}\text{Sr}_{\text{carbonate}}$ chemo-stratigraphy at OST. Diagram including geologic time scale (a), Late Ordovician to Early Silurian (Llandovery) sea level fluctuations (blue shaded area) (b) with related arc activity (red solid line) and weatherability (yellow dotted line) (adapted from refs.^{9,58–60}), columnar section showing the lithology of the target area (c), and plots showing in-situ $\delta^{18}\text{O}_{\text{quartz}}$ and $^{87}\text{Sr}/^{86}\text{Sr}_{\text{carbonate}}$ chemo-stratigraphic results with detrital quartz contents (d), in which lines connect the maximum values of each point and error bars (2σ) are specified. The yellow-shaded area is the Ordovician–Silurian transition (OST) zone based on U–Pb zircon age dating. The gray shaded area is the chemo-stratigraphy for the PBSC unit. In the PBSC unit, an abrupt drop in in-situ $\delta^{18}\text{O}_{\text{quartz}}$ values accompanied by a sharp increase in detrital quartz content, and a rapid change in in-situ $^{87}\text{Sr}/^{86}\text{Sr}_{\text{dolomite}}$ values in the clastic dolomite pebble (fine-grained dolomite aggregate) were observed.

range < 0.7110). However, the trend of all $^{87}\text{Sr}/^{86}\text{Sr}_{\text{calcite}}$ values in the $^{87}\text{Sr}/^{86}\text{Sr}_{\text{calcite}}$ vs. $1/\text{Sr}$ correlation also converged to a value of about 0.7085 (Fig. 4b). This suggests that it is highly likely that the carbonate successions in the study area were also affected by a hydrothermal fluid event after deposition. The calcite in the PBSC unit is cement, and the $^{87}\text{Sr}/^{86}\text{Sr}_{\text{calcite}}$ vs. $1/\text{Sr}$ trend shows a slight difference from the calcite in the carbonate rock units, which seems to be due to the difference in geochemical conditions at the time of each calcite formation (Fig. 4b).

Discussion

Chronology of PBSC unit.

The age of the PBSC unit should be considered comprehensively with the age of the lower and upper carbonate rock units. (1) The age of the upper part of the lower carbonate rock unit was constrained from the latest Middle Ordovician to the earliest Late Ordovician by Hong and Lee²⁵. Considering conodont biostratigraphy by Lee²⁶ and Cheong et al.²⁷, they proposed the age using correlation of carbon isotope based chemo-stratigraphy as an alternative approach due to the lack of a fossil index in this unit. (2) For the age of the PBSC unit, an age frequency graph was presented by combining the highly reliable U–Pb zircon age dating results reported by Jang¹⁸ and the results of several sites in the PBSC unit (Supplementary Fig. 7). (3) In addition, based on Conodont biostratigraphy by Cheong et al.²⁷ and Lee²⁸, the upper carbonate rock unit was considered

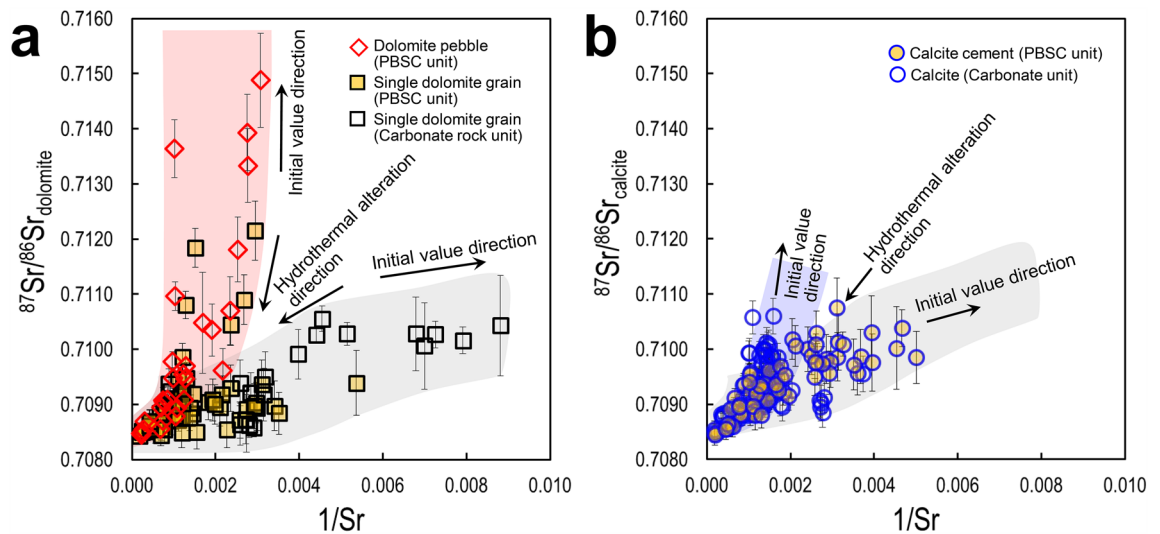


Figure 4. $^{87}\text{Sr}/^{86}\text{Sr}_{\text{carbonate}}$ vs. $1/\text{Sr}$ correlation diagrams. (a) $^{87}\text{Sr}/^{86}\text{Sr}_{\text{dolomite}}$ versus $1/\text{Sr}$ correlation of PBSC and carbonate units. Each trend of clastic dolomite pebble and single dolomite of carbonate units show a distinctly different pathway, and the $^{87}\text{Sr}/^{86}\text{Sr}_{\text{dolomite}}$ values of the two trends converged to about 0.7084. (b) $^{87}\text{Sr}/^{86}\text{Sr}_{\text{calcite}}$ versus $1/\text{Sr}$ correlation of PBSC and carbonate units. The trend of all $^{87}\text{Sr}/^{86}\text{Sr}_{\text{calcite}}$ values also converged to about 0.7085. Each trend of calcite cement in PBSC unit and calcite in carbonate units show a slightly different pathway reflecting the difference in geochemical conditions at the time of creation. Error bars for each point represent 2σ .

a Silurian formation. Considering the above points comprehensively, we constrained the deposition period of the PBSC unit as the OST period.

In the recently reported Conodont Biostratigraphy, the upper part of the lower carbonate rock and PBSC units were suggested as Middle Ordovician (Darriwilian)²⁹, and the upper carbonate rock unit as Upper Ordovician (Sandbian)³⁰. Compared to the results we used in the previous studies and this study mentioned above, there are some conflicting points. Since both detrital dolomite pebbles and single dolomite grains are observed in the microfacies of PBSC units, Middle Ordovician (Darriwilian) conodonts could be sufficiently found in conodonts derived from PBSC units with these characteristics. However, in the conodont study of the upper carbonate rock unit, the species of the previous research group²⁸ and the latest research group³⁰ were not completely matched, and no direct comparison with similar species was presented. The only one mentioned together in both groups was *Panderodus gracilis* (*Panderodus species*), which was one of the dominant species in the upper carbonate rock unit. This species has been reported to have relatively long biostratigraphic ranges (mainly Middle Ordovician to Silurian; Rexroad and Craig³¹). Thus, there is still a prolonged debate about dating by biostratigraphy alone.

We respect conodont-based biostratigraphy as one of the powerful correlation methods. However, we clarify the following points in this study: (1) The age of the upper part of the lower carbonate rock unit was constrained as at least Middle to Late Ordovician based on carbon isotope stratigraphy considering conodont biostratigraphy. (2) The deposition period of the PBSC unit was constrained to the OST period based on the frequency of zircon U–Pb age dating results. (3) The possibility of a detrital conodont could not be ruled out in the carbonate platform undergoing the advent and retreat of a shallow marine environment as the sea level rises and falls. Therefore, the results of zircon age dating, chemo-stratigraphy, and biostratigraphy should be complemented mutually and interpreted comprehensively.

$\delta^{18}\text{O}$ isotope, an indicator for provenance change. In the carbonate rock and PBSC units, the characteristics of quartz, including micro-texture, abundance, and isotope value, are completely distinct.

In the micro-texture of the carbonate rock unit, quartz has fine-sized grains (usually several μm to tens of μm , rarely up to 200 μm), subhedral to anhedral shape, and distal influx characteristics are observed (Fig. 3d; Supplementary Fig. 6). In the micro-texture of the PBSC unit, quartz has various grain sizes (tens to hundreds of μm), poor sorting, subangular shape with poor roundness, and proximal influx characteristics are observed (Fig. 2d and e; Supplementary Figs. 2 and 5).

The quartz abundance of the PBSC unit is closely related to the geological processes that acted on this carbonate platform. The lower carbonate rock unit underwent folding and uplifting by compressive force (Figs. 1 and 5) and formed karst by denudation, weathering, and erosion (Figs. 2g, 3d, and 5; Supplementary Figs. 1 and 4). The exposure of the continental board due to geological events (uplifting, weathering, and erosion) provides sufficient conditions to increase the supply of clasts to the PBSC unit. The decisive event was the increase in the continental free board due to the rapid decrease in sea level during the OST period (Supplementary Fig. 5). This massively increased the amount of clasts that could be deposited. We confirmed a significant influx of terrestrial clasts (especially quartz, dolomite pebble, and dolomite) in both micro-texture observation and quantitative XRD analysis (Fig. 3d).

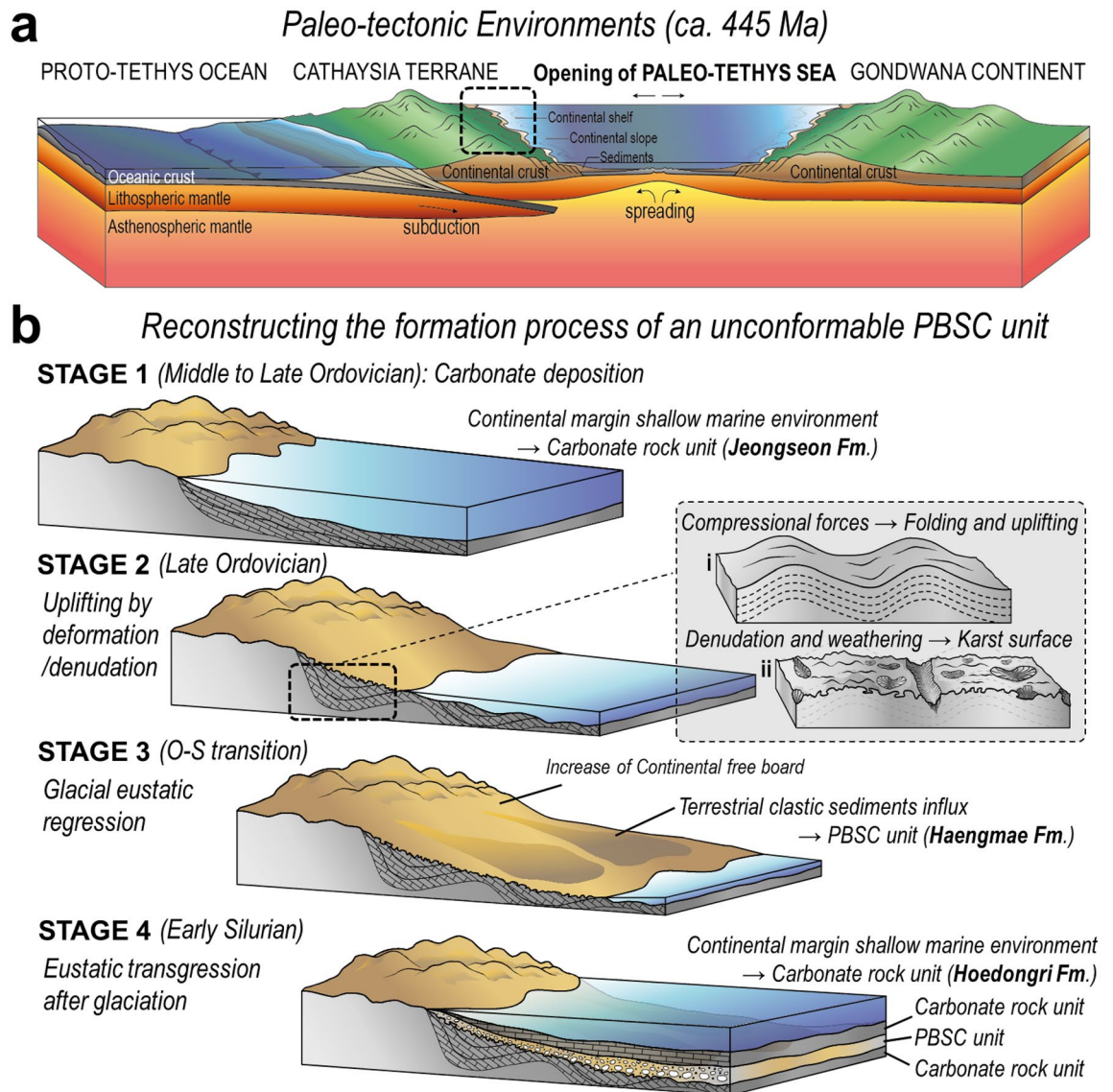


Figure 5. Conceptual illustration of paleo-tectonic environments and paleo-depositional model. **(a)** Conceptual illustration showing the northwest margin of Gondwana at ca. 445 Ma, including the Cathaysia terrane breaking-off from the Gondwana and subsequent Paleotethys Sea opening. **(b)** A proposed depositional model for the PBSC unit creation in the Cathaysia terrane, inferred from its clastic lithology, the unconformable relationship with the lower carbonate unit, in-situ $\delta^{18}\text{O}_{\text{quartz}}$ and $^{87}\text{Sr}/^{86}\text{Sr}_{\text{carbonate}}$ proxies, and the global events during the OST period. Detailed explanations of each stage are described in the text.

Since the quartz in the carbonate rock units was deposited being distal, it is ambiguous to estimate the provenance. However, from the exposed continental board, quartz deposited in the PBSC unit as being proximal has $\delta^{18}\text{O}$ values ranging from 17.55 to 23.65 ‰. Unlike quartz of carbonate rock units, which has a range of 23.56 ~ 27.01 ‰, it strongly indicates that it is a completely different provenance material. The sedimentary structure of the detrital clast unit is very poor and vulnerable to various post-depositional events. Nevertheless, since quartz is very resistant to oxygen isotope exchange²⁰, it preserves the original oxygen isotope value. It is largely unaffected by post-depositional alterations such as intense weathering and denudation. Therefore, in-situ $\delta^{18}\text{O}_{\text{quartz}}$ considering the micro-texture and content characteristics of quartz is a useful proxy as an indicator of provenance change before and after OST.

$^{87}\text{Sr}/^{86}\text{Sr}$ isotope, a geochemical indicator for syn-/post-depositional event. We found records of different geochemical conditions from the Sr isotope values of carbonate minerals (calcite and dolomite) by attempting in-situ mineral analysis (Figs. 3d and 4). There are two things to note here: First, two trends are evident in the $^{87}\text{Sr}/^{86}\text{Sr}_{\text{dolomite}}$ value of carbonate rock and PBSC units (Fig. 4a). Considering the characteristics of the PBSC unit, a significantly fluctuating $^{87}\text{Sr}/^{86}\text{Sr}$ ratio and relatively high Sr composition were confirmed in single dolomite grain and dolomite pebble. This means that dolomite with syn-depositional values under different geochemical conditions was introduced into the PBSC unit. Second, the $^{87}\text{Sr}/^{86}\text{Sr}$ isotope value converges to

a specific value (ca. 0.7084) under the influence of hydrothermal alteration as a post-depositional event. A PBSC unit is a typical clastic rock unit. Compared to the lower and upper carbonate rock units, this unit shows porous characteristics in both macro and micro scales (Fig. 2a; Supplementary Fig. 2). Because of this, after the syn-depositional event, this unit could act as a channel for hydrothermal fluid flowing from the fault zone (Fig. 1c; Supplementary Fig. 1c). Park et al.¹⁹ reported phengite with muscovite–celadonite solid solution relationship as evidence of hydrothermal fluid introduced into the syn-sedimentary growth-fault in the PBSC unit. In micro-texture, phengite is observed in crystalline and pore-filling types, which are fluid-filled, not detrital.

The value of $^{87}\text{Sr}/^{86}\text{Sr}$ records both syn-depositional and post-depositional geochemical conditions. There are many factors that affect $^{87}\text{Sr}/^{86}\text{Sr}$ ^{14,21}, and the causes have been proposed as follows. Potential causes of increase include (1) diagenetic alteration, (2) contamination from detrital siliciclastic; Potential causes of the decrease include (1) increased rates of seafloor spreading and hydrothermal activity that provided a higher input of non-radiogenic Sr to the ocean (2) hydrothermal activity, (3) eustatic sea level rise that flooded radiogenic source area, increased weathering rates of volcanic rock, (4) ocean ventilation, non-radiogenic Sr reservoir. Based on this, in our study, the detrital clastic unit, PBSC, has a higher initial value than the $^{87}\text{Sr}/^{86}\text{Sr}_{\text{dolomite}}$ value of the carbonate rock unit, which means that it is derived from completely different geochemical conditions at the time of syn-deposition. In this carbonate platform, the $^{87}\text{Sr}/^{86}\text{Sr}$ value follows a decreasing trend (hydrothermal alteration trend) due to the Sr exchange of carbonate mineral under the influence of hydrothermal fluid after deposition. Therefore, the $^{87}\text{Sr}/^{86}\text{Sr}$ isotope of carbonate minerals is a useful proxy as a geochemical indicator of syn-/post-depositional events.

Depositional model for the PBSC unit creation. Summarizing the characteristics of the PBSC unit, the unit (1) shows typical terrestrial clastic lithology characteristics, (2) has an angular unconformity relationship with the lower carbonate unit, (3) was temporally formed at the time of the Ordovician–Silurian transition, (4) was spatially located in the Cathaysia terrane of the Gondwana Supercontinent. Therefore, it is clear that these characteristics of the PBSC unit are closely related to the geological events that occurred in the Gondwana during the OST period. The most representative geological events are the Paleo-Tethys Sea opening and global glacial eustatic regression. In particular, in the PBSC unit, which has an age constraint as an OST period, the continental free board increased according to the abrupt drop in sea level, resulting in a large amount of terrestrial clasts influx. By linking these geological events with the clastic lithology and in-situ isotope chemo-stratigraphic characteristics of the PBSC unit, it can be inferred that the PBSC unit was formed through the following steps (Fig. 5).

Stage-1: Sedimentation of a carbonate unit (Jeongseon Fm.) begins in the Middle Ordovician period in the shallow marine environment of the terrestrial margin formed by the break-up of the Cathaysia terrane from the Gondwana.

Stage-2: During the Late Ordovician period, the separation of the Cathaysia terrane and the subsequent opening of the Paleo-Tethys Sea was in full swing, and as plate movement occurred on the opposite side of the Cathaysia terrane, the southeastern Cathaysia margin was placed under a compressional condition from both sides. This causes deformation and uplifting of the carbonate unit (Jeongseon Fm.) deposited in the Cathaysia terrane (Stage-2i), and is exposed to the surface and denuded by weathering to create the Karst surface (Stage-2ii).

Stage-3: The eustatic sea-level regression by the global glaciation maximum in the Latest Ordovician period leads to an increase in continental exposure during the OST period, and a large amount of terrestrial clasts produced by erosion occurs. These cover the Karst surface of the carbonate unit and form an unconformable PBSC unit.

Stage-4: As the global glaciation ends in the Silurian period, the top of the PBSC unit turns into a shallow marine environment again through gradual eustatic transgression, and the deposition of another carbonate unit (Hoedongri Fm.) begins. Subsequent geological processes cause various alterations to the relatively porous PBSC unit and precipitate secondary minerals (dolomite, phengite, and calcite cement).

In conclusion, the formation process model of the PBSC unit in the Cathaysia terrane region can be a criterion to explain the clastic sedimentary succession created in each continent during the OST period.

Methods

Sample preparation. Several field works were conducted from November 2019 to April 2023 in the Taebaeksan Basin of the Republic of Korea (South Korea). Based on the structural, sedimentological, and mineralogical characteristics of the traceable PBSC and carbonate rock unit, mapping was performed and a geological map was drawn (Supplementary Fig. 1). All PBSC and carbonate rock samples were polished as slabs, thin sections, and epoxy mounts. Polishing was conducted in several steps, starting at 20 μm and finishing at 0.25 μm . Mineralogical and micro-textural characteristics were examined using a polarizing microscope and SEM–EDS with a back-scattered Electron (BSE) detector high-vacuum (HV) SEM (JSM-5610LV; JEOL Ltd., Tokyo, Japan) and an EDS system (Oxford Instruments, Abingdon, UK) at Yonsei University, Seoul, South Korea. In order to apply the in-situ method to isotope analysis, a route map was created to confirm the distribution and texture of the target mineral with merging compo images.

In-situ oxygen isotope analyses of quartz minerals. A total of 313 (including reference data) in-situ oxygen isotope analyses of quartz minerals were performed with LG-SIMS (CAMECA IMS1300-HR³ Large-Geometry SIMS) from KBSI (Ochang, South Korea). On the Au-coated epoxy mount surface with a thickness of 20 nm, $\delta^{16}\text{O}_{\text{quartz}}$ and $\delta^{18}\text{O}_{\text{quartz}}$ signals were obtained from the core to the rim of the grain with a 10 μm spot beam size. The signal was obtained in 20 cycles, and the measurement time was about 7–8 min. As a reference material, Unil-Q³², natural crystals of quartz from Chile, provided by Lausanne University, was used. In this

study, the in-situ $\delta^{18}\text{O}_{\text{quartz}}$ value of Unil-Q was $9.8564 \pm 0.2604\%$ (2 s), which has high reliability and reproducibility. Raw data and calculated $\delta^{18}\text{O}_{\text{quartz}}$ values are reported in Supplementary Table 3.

In-situ strontium isotope analyses of carbonate minerals. A total of 591 (including reference data) in-situ strontium isotope analyses of carbonate minerals were performed with LA-MC-ICP-MS (Nu Plasma II MC-ICP-MS with NWR 193uc laser system) from KBSI (Ochang, South Korea). Calcite cement, dolomite grains, and dolomite pebbles were targeted and analyzed with the following ablation conditions: 100 μm spot beam size of single hole drilling ablation mode, 30 secs dwell time, and a fluence of $\sim 4.0 \text{ J/cm}^2$. The $^{87}\text{Sr}/^{86}\text{Sr}$ value of the reference material (KRNC-1) is 0.708604 ± 0.000022 , which has high reliability and reproducibility. Reference material, NIST, and calculated $^{87}\text{Sr}/^{86}\text{Sr}$ of carbonate mineral (calcite, dolomite) values are reported in Supplementary Table 4.

X-ray diffraction with RIR method. A total of 66 powdered bulk rock samples were analyzed with the Rigaku Miniflex II X-ray Diffraction (XRD) system from Yonsei University. All rock samples were ground into fine-sized powder using a mortar and pestle, and mixed homogeneously with a corundum (Al_2O_3) powder in a weight ratio of 1:1. With the prepared powder samples, the XRD system was performed under $\text{CuK}\alpha$ radiation, step-scan mode 0.02° step, 1 s/step scanning time, and $2\text{--}55^\circ$ 2θ ranges conditions using a 6-sample holder. Semi-quantitative analysis of mineral composition was conducted with the Reference Intensity Ratio (RIR) method^{33–37}. From the results of X-ray diffraction analysis, the ratio of peak intensities of corundum and major minerals (calcite, dolomite, quartz, illite, etc.) was determined. Quantitative values were then calculated using the theoretical RIR values. The quantitative analysis results for major minerals are presented in Supplementary Table 2, and among the data, the results for quartz are shown in Fig. 3d.

Zircon U–Pb age dating. The PBSC unit rock sample was crushed and the heavy mineral concentrate obtained by the heavy liquid separation process was obtained. The zircon grains were handpicked through a stereoscopic microscope. The separated zircon grains were mounted in epoxy resin with a reference zircon. After polishing the mount, analytical points were considered by observing the micro-texture with SEM-BSE. U–Pb age dating was performed using a Nu Plasma II multi-collector inductively coupled plasma mass spectrometry (LA-MC-ICP-MS) instrument equipped with a New Wave Research 193-nm ArF excimer laser ablation system at the KBSI (Korea Basic Science Institute). All analyses were conducted with a spot size of 15 μm , a repetition rate of 5 Hz, and an energy density of 4.5 J/cm^2 . The background intensity time of 30 secs, dwell time of 30 secs, and washout time of 20 secs were set. As reference zircons, 91,500 and Plesovice^{38,39} were used. All age values were calculated after data reduction using Iolite^{40,41} and Isoplot⁴² softwares. Frequency histogram of detrital zircon U–Pb age dating for PBSC unit (Haengmae Fm.) integrating unpublished data (In this study) using LA-MC-ICP-MS and the results of previous results^{17,18} using LA-MC-ICP-MS and SHRIMP is presented in Supplementary Fig. 7. Raw data is reported in Supplementary Table 5.

Data availability

The authors confirm that the data supporting the findings of this study are available within the article and its supplementary materials.

Received: 17 May 2023; Accepted: 6 September 2023

Published online: 13 September 2023

References

- Fan, J. X. *et al.* A high-resolution summary of Cambrian to Early Triassic marine invertebrate biodiversity. *Science* **367**, 272–277. <https://doi.org/10.1126/science.aax4953> (2020).
- Finnegan, S. *et al.* The magnitude and duration of Late Ordovician–Early Silurian glaciation. *Science* **331**, 903–906. <https://doi.org/10.1126/science.1200803> (2011).
- Melchin, M. J., Mitchell, C. E., Holmden, C. & Štorch, P. Environmental changes in the Late Ordovician–early Silurian: Review and new insights from black shales and nitrogen isotopes. *Geol. Soc. Am. Bull.* **125**, 1635–1670. <https://doi.org/10.1130/B30812.1> (2013).
- Ghienne, J. F. *et al.* A Cenozoic-style scenario for the end-Ordovician glaciation. *Nature Commun.* **5**, 4485. <https://doi.org/10.1038/ncomms5485> (2014).
- Jing, X. *et al.* Ordovician–Silurian true polar wander as a mechanism for severe glaciation and mass extinction. *Nat. Commun.* **13**, 7941. <https://doi.org/10.1038/s41467-022-35609-3> (2022).
- Qiu, Z. *et al.* A nutrient control on expanded anoxia and global cooling during the Late Ordovician mass extinction. *Commun. Earth Environ.* **3**, 82. <https://doi.org/10.1038/s43247-022-00412-x> (2022).
- Scotese, C. R. Plate tectonic evolution during the last 1.5 billion years: the movie. Paper presented at the Geological Society of America Annual Meeting, Indianapolis, IN, Nov. 5, <https://doi.org/10.1130/abs/2018AM-320136> (2018).
- Scotese, C. R. An atlas of phanerozoic paleogeographic maps: The seas come in and the seas go out. *Annu. Rev. Earth. Planet. Sci.* **49**, 679–728. <https://doi.org/10.1146/annurev-earth-081320-064052> (2021).
- Cocks, L. R. M. & Torsvik, T. H. Ordovician palaeogeography and climate change. *Gondwana Res.* **100**, 53–72. <https://doi.org/10.1016/j.gr.2020.09.008> (2021).
- Clayton, R. N., Rex, R. W., Syers, J. K. & Jackson, M. L. Oxygen isotope abundance in quartz from Pacific pelagic sediments. *J. Geophys. Res.* **77**, 3907–3915. <https://doi.org/10.1029/JC077i021p03907> (1972).
- Mizota, C., Kusakabe, M. & Noto, M. Oxygen isotope compositions of fine-grained quartz from soils and sediments in Southern Shizuoka. *Central Japan. Geochem. J.* **22**, 33–40. <https://doi.org/10.2343/geochemj.22.33> (1988).
- Smith, M. A. & Pell, S. Oxygen-isotope ratios in quartz as indicators of the provenance of archaeological ochres. *J. Archaeol. Sci.* **24**, 773–778. <https://doi.org/10.1006/jasc.1996.0159> (1997).
- Hou, S., Yang, S., Sun, J. & Ding, Z. Oxygen isotope compositions of quartz grains (4–16 μm) from Chinese eolian deposits and their implications for provenance. *Sci. China Series D-Earth Sci.* **46**, 1003–1011. <https://doi.org/10.1007/BF02959395> (2003).

14. Edwards, C. T. *et al.* Strontium isotope ($^{87}\text{Sr}/^{86}\text{Sr}$) stratigraphy of Ordovician bulk carbonate: Implications for preservation of primary seawater values. *Geol. Soc. Am. Bull.* **127**, 1275–1289. <https://doi.org/10.1130/B31149.1> (2015).
15. Chough, S. K., Kwon, S. T., Ree, J. H. & Choi, D. K. Tectonic and sedimentary evolution of the Korean peninsula: a review and new view. *Earth Sci Rev.* **52**, 175–235. [https://doi.org/10.1016/S0012-8252\(00\)00029-5](https://doi.org/10.1016/S0012-8252(00)00029-5) (2000).
16. Lee, H. S. & Chough, S. K. Sequence stratigraphy of Pyeongan Supergroup (Carboniferous–Permian), Taebaek area, mid-east Korea. *Geosci. J.* **10**, 369–389. <https://doi.org/10.1007/BF02910433> (2006).
17. Kim, N. *et al.* Distribution and stratigraphical significance of the haengmae formation in Pyeongchang and Jeongseon areas. *South Korea. Econ. Environ. Geol.* **53**, 383–395. <https://doi.org/10.9719/EEG.2020.53.4.383> (2020).
18. Jang, Y. Structural style of the Phanerozoic polyphase orogenic belt in the western Taebaeksan Zone, Okcheon Belt, Korea: Insights from multidisciplinary analyses: Doctoral dissertation, Ph. D. Thesis, Yonsei University, 1–220; <https://library.yonsei.ac.kr/search/detail/CAT000001892590?briefLink=/main/searchBrief?q=Structural+style+of+the+Phanerozoic+polyphase+orogenic+belt+in+the+western+Taebaeksan+Zone%2C+Okcheon+Belt%2C+Korea%3A+Insights+from+multidisciplinary+analyses#> (2017).
19. Park, C., Kim, N., Choi, S. & Song, Y. Mg-phengite in carbonate rock syngenetically formed from hydrothermal fluid: Micro-textural evidence and mineral chemistry. *Minerals* **10**, 668–681. <https://doi.org/10.3390/min10080668> (2020).
20. Vennemann, T. W., Kesler, S. E. & O'Neil, J. R. Stable isotope compositions of quartz pebbles and their fluid inclusions as tracers of sediment provenance: Implications for gold-and uranium-bearing quartz pebble conglomerates. *Geology* **20**, 837–840. [https://doi.org/10.1130/0091-7613\(1992\)020%3c0837:SICOQP%3e2.3.CO;2](https://doi.org/10.1130/0091-7613(1992)020%3c0837:SICOQP%3e2.3.CO;2) (1992).
21. Montañez, I. P. *et al.* Integrated Sr isotope variations and sea-level history of Middle to Upper Cambrian platform carbonates: Implications for the evolution of Cambrian seawater $^{87}\text{Sr}/^{86}\text{Sr}$. *Geology* **24**, 917–920. [https://doi.org/10.1130/0091-7613\(1996\)024%3c0917:ISIVAS%3e2.3.CO;2](https://doi.org/10.1130/0091-7613(1996)024%3c0917:ISIVAS%3e2.3.CO;2) (1996).
22. Montañez, I. P. *et al.* Evolution of the Sr and C isotope composition of Cambrian oceans. *GSA Today* **10**, 1–7 (2000).
23. Paytan, A. *et al.* A 35-million-year record of seawater stable Sr isotopes reveals a fluctuating global carbon cycle. *Science* **371**, 1346–1350. <https://doi.org/10.1126/science.aaz9266> (2021).
24. Wang, J. *et al.* The evolution of the marine carbonate factory. *Nature* **615**, 265–269. <https://doi.org/10.1038/s41586-022-05654-5> (2023).
25. Hong, S. K. & Lee, Y. I. Geological age of the Jeongseon formation, Joseon supergroup (lower Paleozoic): a perspective from carbon isotope stratigraphy. *Geosci. J.* **11**, 1–9. <https://doi.org/10.1007/BF02910376> (2007).
26. Lee, H. Y. Conodonts from the Maggol- and the Jeongseon Formation (Ordovician), Kangweon-Do. *South Korea. J. Geol. Soc. Korea.* **12**, 151–181 (1976).
27. Cheong, C. H., Lee, H. Y., Ko, I. S. & Lee, J. D. A study on stratigraphy and sedimentological environments of the lower Paleozoic sequences in South Korea. *J. Natl. Academy Sci. Republ. Korea* **18**, 123–159 (1979).
28. Lee, H. Y. Discovery of Silurian Conodont Fauna from South Korea. *J. Geol. Soc. Korea.* **16**, 114–123 (1980).
29. Lee, B. S. Conodonts from the 'Lower Limestone' and Haengmae Formation in western Jeongseon, Korea and their implication for lithostratigraphic correlation. *Geosci. J.* **24**, 113–120. <https://doi.org/10.1007/s12303-019-0034-7> (2020).
30. Lee, B. S. Upper ordovician (Sandbian) conodonts from the Hoedongri formation of western Jeongseon. *Korea. Geosci. J.* **23**, 695–705. <https://doi.org/10.1007/s12303-019-0009-8> (2019).
31. Rexroad, C. B., & Craig, W. W. Restudy of conodonts from the Bainbridge Formation (Silurian) at Lithium, Missouri. *J. Paleontol.* **684**–703; <https://www.jstor.org/stable/1302806> (1971).
32. Seitz, S. *et al.* Quartz reference materials for oxygen isotope analysis by SIMS. *Geostand Geoanal. Res.* **41**, 69–75. <https://doi.org/10.1111/ggr.12133> (2017).
33. Hubbard, C. R., Evans, E. H. & Smith, D. K. The reference intensity ratio, I/I_c, for computer simulated powder patterns. *J. Appl. Crystallogr.* **9**, 169–174. <https://doi.org/10.1107/S0021889876010807> (1976).
34. Hubbard, C. R. & Snyder, R. L. RIR-measurement and use in quantitative XRD. *Powder Diffr.* **3**, 74–77. <https://doi.org/10.1017/S0885715600013257> (1988).
35. Snyder, R. L. The use of reference intensity ratios in X-ray quantitative analysis. *Powder Diffr.* **7**, 186–193. <https://doi.org/10.1017/S0885715600018686> (1992).
36. Al-Jaroudi, S. S., Ul-Hamid, A., Mohammed, A. R. I. & Saner, S. Use of X-ray powder diffraction for quantitative analysis of carbonate rock reservoir samples. *Powder Technol.* **175**, 115–121. <https://doi.org/10.1016/j.powtec.2007.01.013> (2007).
37. Park, C., Kim, H. & Song, Y. Mineralogical, micro-textural, and geochemical characteristics for the carbonate rocks of the lower Makgol Formation in Seokgaegae section. *Econ. Environ. Geol.* **51**, 323–343. <https://doi.org/10.9719/EEG.2018.51.4.323> (2018).
38. Wiedenbeck, M. *et al.* Three natural zircon standards for U-Th-Pb, Lu-Hf, trace element and REE analyses. *Geostand. Newsl.* **19**, 1–23. <https://doi.org/10.1111/j.1751-908X.1995.tb00147.x> (1995).
39. Sláma, J. *et al.* Plešovice zircon—a new natural reference material for U-Pb and Hf isotopic microanalysis. *Chem. Geol.* **249**, 1–35. <https://doi.org/10.1016/j.chemgeo.2007.11.005> (2008).
40. Paton, C. *et al.* Improved laser ablation U-Pb zircon geochronology through robust downhole fractionation correction. *Geochem. Geophys. Geosystems.* **11**, 1–36. <https://doi.org/10.1029/2009GC002618> (2010).
41. Paton, C. *et al.* Lolite: Freeware for the visualisation and processing of mass spectrometric data. *J. Anal. At. Spectrom.* **26**, 2508–2518. <https://doi.org/10.1039/C1JA10172B> (2011).
42. Ludwig, K. Users Manual for ISOPLOT 3.6: A geochronological toolkit for Microsoft Excel: Special Publication 4, Berkeley Geochronology Center, University of California at Berkeley (revision of April 8, 2008), (2008).
43. Hurst, J. M. & Surlyk, F. Tectonic control of Silurian carbonate-shelf margin morphology and facies, North Greenland. *AAPG Bull.* **68**, 1–17. <https://doi.org/10.1306/AD460959-16F7-11D7-8645000102C1865D> (1984).
44. Smith, P. & Moseley, G. The karst and palaeokarst of North and North-East Greenland—physical records of cryptic geological intervals. *GEUS B.* **49**, 1–23. <https://doi.org/10.34194/geusb.v49.8298> (2022).
45. Pollock, J. C., Wilton, D. H. C., Van Staal, C. R. & Morrissey, K. D. U-Pb detrital zircon geochronological constraints on the Early Silurian collision of Ganderia and Laurentia along the Dog Bay Line: The terminal Iapetan suture in the Newfoundland Appalachians. *Am. J. Sci.* **307**, 399–433. <https://doi.org/10.2475/02.2007.04> (2007).
46. Castonguay, S. *et al.* Ordovician and Silurian metamorphic cooling ages along the Laurentian margin of the Quebec Appalachians: Bridging the gap between New England and Newfoundland. *Geology* **25**, 583–586. [https://doi.org/10.1130/0091-7613\(1997\)025%3c0583:OASMCA%3e2.3.CO;2](https://doi.org/10.1130/0091-7613(1997)025%3c0583:OASMCA%3e2.3.CO;2) (1997).
47. Dronov, A. Late Ordovician cooling event: evidence from the Siberian Craton. *Palaeogeogr. Palaeoclimatol. Palaeoecol.* **389**, 87–95. <https://doi.org/10.1016/j.palaeo.2013.05.032> (2013).
48. Kanygin, A. V. *et al.* Ordovician of the Siberian platform, In: Finney, S. C., and Berry W. B. N. (Eds.), The Ordovician system. *Geol. Soc. Am. Spec. Pap.* **466**, 105–117; [https://doi.org/10.1130/2010.2466\(07\)](https://doi.org/10.1130/2010.2466(07)) (2010).
49. Antoshkina, A. I. Late ordovician-Early Silurian facies development and environmental changes in the Subpolar Urals. *Lethaia* **41**, 163–171. <https://doi.org/10.1111/j.1502-3931.2008.00111.x> (2008).
50. Tuuling, I. & Flodén, T. Late Ordovician carbonate buildups and erosional features northeast of Gotland, northern Baltic Sea. *GFF* **122**, 237–249. <https://doi.org/10.1080/11035890001222237> (2000).
51. Zheng, B. *et al.* Nature of the late ordovician-early silurian xiaohu section, Hunan-Hubei area, South China: Implications for the Kwangsi orogeny. *Int. Geol. Rev.* **62**, 1262–1272. <https://doi.org/10.1080/00206814.2019.1644541> (2020).

52. Yu, T. *et al.* Provenance of late ordovician sedimentary rocks in the SE Yangtze block: Implications for deposition in an active continental margin. *Ore Geol. Rev.* **127**, 1–16. <https://doi.org/10.1016/j.oregeorev.2020.103862> (2020).
53. Liu, J. *et al.* Palaeogeomorphology and its control on the development of sequence stratigraphy and depositional systems of the Early Silurian in the Tarim Basin. *Pet. Sci.* **7**, 311–322. <https://doi.org/10.1007/s12182-010-0073-1> (2010).
54. Liu, J. *et al.* Detrital zircon U-Pb geochronology and its provenance implications on Silurian Tarim basin. *J. Earth Sci.* **23**, 455–475. <https://doi.org/10.1007/s12583-012-0268-z> (2012).
55. Doner, Z., Kumral, M., Demirel, I. H. & Hu, Q. Geochemical characteristics of the Silurian shales from the central Taurides, southern Turkey: Organic matter accumulation, preservation and depositional environment modeling. *Mar. Pet. Geol.* **102**, 155–175. <https://doi.org/10.1016/j.marpetgeo.2018.12.042> (2019).
56. Casas, J. M. Ordovician deformations in the Pyrenees: New insights into the significance of pre-Variscan ('sardic') tectonics. *Geol. Mag.* **147**, 674–689. <https://doi.org/10.1017/S0016756809990756> (2010).
57. Halpern, K. & Carrera, M. G. Post-glacial Hirnantian (Upper Ordovician) bryozoans from western Argentina: implications for survival and extinction patterns. *Ameghiniana* **51**, 243–253. <https://doi.org/10.5710/AMGH.20.03.2014.1840> (2014).
58. Domeier, M., Magni, V., Hounslow, M. W. & Torsvik, T. H. Episodic zircon age spectra reflect true fluctuations in global subduction. *Sci. Rep.* **8**, 1–9. <https://doi.org/10.1038/s41598-018-35040-z> (2018).
59. Rasmussen, C. M., Kröger, B., Nielsen, M. L. & Colmenar, J. Cascading trend of Early Paleozoic marine radiations paused by Late Ordovician extinctions. *Proc. Natl. Acad. Sci. U.S.A.* **116**, 7207–7213. <https://doi.org/10.1073/pnas.182112311> (2019).
60. Torsvik, T. H. *et al.* Connecting the deep Earth and the atmosphere, In: Marquardt, H., Ballmer, M.D., Cottaar, S., and Konter, J.G. (Eds.), *Mantle Convection and Surface Expressions*, AGU Monograph (in press), (2020).

Acknowledgements

We wish to extend special thanks to editors and anonymous reviewers for their constructive and thoughtful comments. Also, we especially thanks to Dr. Choi (Woohyun Choi, Kyungpook National University) for assistance with the sketch of Fig. 2g. This study was funded by the National Research Foundation of Korea under Grant NRF 2018R1D1A1B07051418. This research was supported in part by the IiKSNF and KETEP grant funded by the Korean government MOTIE (No.2021040101003B) to S.K.

Author contributions

C.P. (first author) and Y.S. (corresponding author; yungoo@yonsei.ac.kr): Contributed to developing the concept, performing field survey, analyzing data, interpreting data, generating figures, and writing manuscript. C.P., Y.S., N.K., S.J.C., U.C., Y.J. and S.K.: Contributed to performing field survey and interpreting data. C.P. and J.K.: Contributed to analyzing in-situ oxygen isotope. C.P., H.K., and Y.J.J.: Contributed to analyzing in-situ strontium isotope.

Competing interests

The authors declare no competing interests.

Additional information

Supplementary Information The online version contains supplementary material available at <https://doi.org/10.1038/s41598-023-42200-3>.

Correspondence and requests for materials should be addressed to Y.S.

Reprints and permissions information is available at www.nature.com/reprints.

Publisher's note Springer Nature remains neutral with regard to jurisdictional claims in published maps and institutional affiliations.



Open Access This article is licensed under a Creative Commons Attribution 4.0 International License, which permits use, sharing, adaptation, distribution and reproduction in any medium or format, as long as you give appropriate credit to the original author(s) and the source, provide a link to the Creative Commons licence, and indicate if changes were made. The images or other third party material in this article are included in the article's Creative Commons licence, unless indicated otherwise in a credit line to the material. If material is not included in the article's Creative Commons licence and your intended use is not permitted by statutory regulation or exceeds the permitted use, you will need to obtain permission directly from the copyright holder. To view a copy of this licence, visit <http://creativecommons.org/licenses/by/4.0/>.

© The Author(s) 2023